MODE I AND MODE II FRACTURE BEHAVIOUR OF CARBON/GLASS HYBRID FILAMENT-WOUND RESIN TRANSFER MOULDED COMPOSITES

J. M. Taylor[a*], S. Frenz[b], C. Canturri[c], S. Giannis[b], E. S. Greenhalgh[c]

[a]*Rolls-Royce Plc., PO Box 31 Moor Lane, Derby, DE24 8BJ, UK*
[b]*Element Materials Technology Ltd., Wilbury Way, Hitchin, SG4 0TW, UK*
[c] *Aeronautics, Imperial College London, SW7 2AZ, UK*
**jonathan.taylor@rolls-royce.com*

Keywords: Fracture, epoxy, hybrid

Abstract
This paper describes the results of an investigation into the Mode I and Mode II fracture behaviour of carbon/glass hybrid filament-wound RTM composite materials. The aims of the work were to define the fracture properties of such materials for component design and to investigate the active fracture mechanisms. Mode I and Mode II fracture tests were performed using the difference in layup angle across the crack as the independent variable. The behaviour of the material was observed during the tests and subsequently characterised using optical and scanning electron microscopy. It was found that different fracture mechanisms were active compared to prepreg materials. Inspection of the fracture morphologies showed misalignment of the fibres with the crack driving forces had induced additional fracture processes as compared to those observed at unidirectional ply interfaces.

1. Introduction

1.1 Background and motivation

In the design of gas turbine engines for aircraft the nosecone component, which exists to improve inlet aerodynamics, must have strength to withstand both the fatigue loading from cyclic operation of the engine and impact loading from foreseeable threats.

These requirements can be met in many different ways, but one advantageous construction consists of a cone which is filament-wound using carbon and glass tows on a solid mandrel and subsequently infiltrated with epoxy resin to form a robust shape. This construction method improves damage resistance compared to a glass prepreg construction by changing the failure mode from a small localised delamination and severe back-face fibre failure to a larger diffuse delamination with no back-face fibre failure. This change preserves the hoop continuity and centrifugal load-carrying capability of the structure after impact loading.

1.2 Present work

One critical parameter arising from the filament-wound construction method is that of a variable ‘interply angle’ or the angle difference between adjacent tow layers. This varies

constantly throughout the manufactured component. Therefore, a range of interply angles was studied from 5° (±2.5°) to 60° (±30°). Tests were performed using the double cantilever beam (DCB) and end-loaded split (ELS) test methods using mid-plane PTFE inserts to simulate pre-existing cracks. Investigation of the fracture surfaces was then performed using optical and scanning electron microscopy in order to investigate the fracture processes active in the two loading modes.

2. Specimen design and manufacture

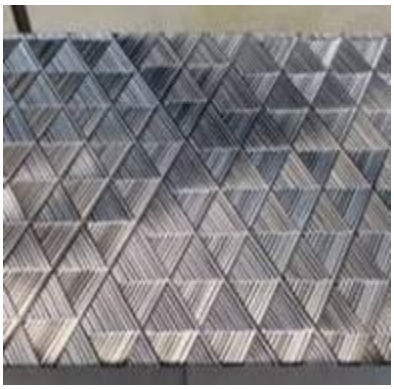

(a)

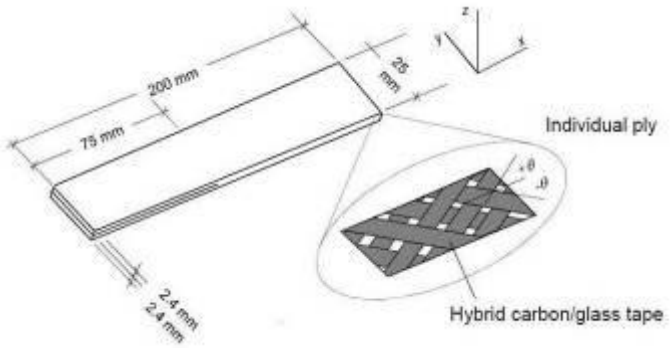

(b)

Figure 1. (a) Example of a filament-wound plate from which DCB and ELS specimens were manufactured, **(b)** geometry of resulting specimens

Test specimens were manufactured by filament winding. In order to create flat plates, the mandrel used for winding was an aluminium plate across which multiple specimens were wound in one plate. An example of a wound plate and a drawing of the finished specimen are shown in Figure 1. The materials used were a standard-modulus epoxy-sized carbon fibre 6k tow, an S-2 glass 6k tow, and a low-viscosity untoughened epoxy RTM matrix. All materials used were standard aerospace-grade materials supplied by the manufacturers. The dimensions of the final cut specimens were 200mm×25mm×4.8mm. A PTFE insert was applied at one end, extending 75mm into the specimen.

3. Test methods

3.1 Mode I testing

The DCB tests were conducted following the principles of ASTM D5528. Owing to issues connected with deviations from a single linear crack front in DCB testing of multi-directional laminates [1] [2], the values of G_{Ic} calculated by modified beam theory equations are not entirely accurate and will be deemed apparent G_{Ic} in this work. Five tests per interply angle were carried out with delamination initiating from the insert. The analysis of all the static test results was initially performed using the Modified Beam Theory (MBT), where the interlaminar fracture toughness, G_{Ic}, can be calculated from Equation 1.

$$G_{Ic} = \frac{3P_c\delta_c}{2b(a+|\Delta_I|)}F \tag{1}$$

where, a is the delamination length, b is the specimen width, P_c the critical load at fracture and δ_c the corresponding critical displacement at fracture. Parameter Δ_I is called the delamination correction length (in mm) and accounts for the beam not being perfectly built-in

(that is, rotation may occur at the delamination front) and the shear deformation at the root of the beam.

3.2 Mode II testing

The End-Loaded Split (ELS) tests were conducted following the procedures described in ESIS Protocol [3]. Regarding the evaluation of the Mode II fracture toughness for these multi-directional laminates, the same limitations apply as with the Mode I testing and fracture toughness. Thus, the evaluated fracture toughness will be termed as apparent G_{IIc}. For all specimens, the clamp length, L, was set to 80 mm. Apparent G_{IIc} is given by Equation 2:

$$G_{IIc} = \frac{9P^2 a_c^{\,2}}{4b^2 h^3 E_1} \cdot F \tag{2}$$

Where P is the applied load, a_c the effective crack length, b and h the width and thickness of the specimen, and E_1 the specimen bending modulus. The parameter F was used in Equation 2 to correct for large displacement effects as indicated in [4]. For both Mode I and Mode II loading conditions modified beam theory was employed for the calculation of the apparent G_c at initiation of delamination growth, from the film insert. Since for most of the cases studied in this work, delamination growth never reached a steady state appearing as a plateau in G_c, the area method was also used to evaluate the average G_c during propagation.

3.3 Post experiment

Following testing the specimens were peeled open to expose the fracture surfaces which were then photographed using a flatbed scanner at 7000dpi. Selected specimens were then cut with a dry diamond saw to expose the fracture surfaces. The matching fracture surfaces were then mounted on aluminium stubs using conductive adhesive, cleaned with dry air and gold sputter coated. Following this, the specimens were examined using a Hitachi S3700N-II scanning electron microscope using 10 kV acceleration voltage.

4. Experimental results

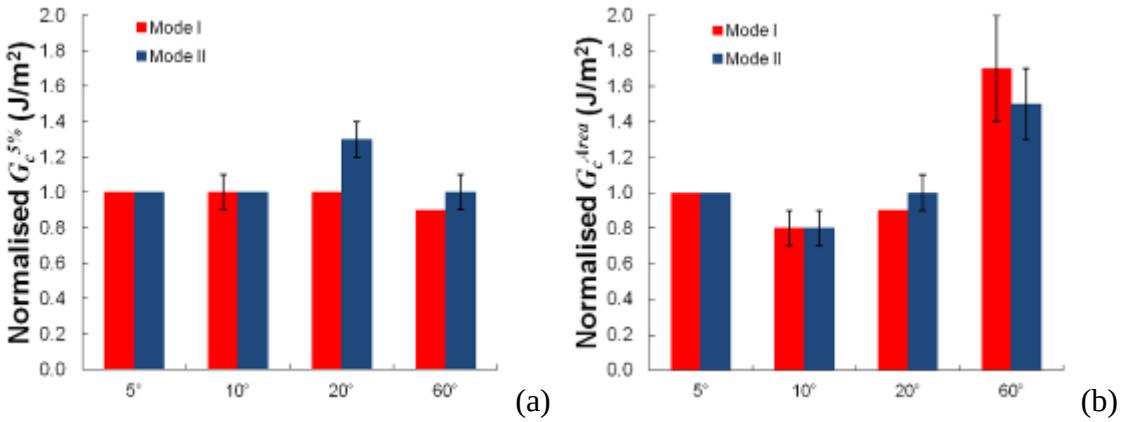

Figure 2 Normalised apparent fracture toughness at **(a)** initiation of delamination growth and **(b)** during propagation for the various interply angles

The experimentally obtained results of the apparent fracture toughness normalised to the mean fracture toughness at 5° interply angle are presented in Figure 2, both for initiation of delamination and growth. For Mode I loading, delamination initiated and propagated in a

stable manner in most cases. The apparent G_c at initiation was found to be nearly unaffected by the interply angle employed, while there was an notable increase in the values of G_c for propagation. In all cases an increasing R-curve was recorded, which is typical when fibre bridging or delamination branching occurs under Mode I loading. The steeper the increase of the delamination resistance curve the more pronounced is the effect of fibre bridging and delamination branching [5]. The initial slopes of the R-curves were found to be very similar for the specimens with 5°, 10° and 20° interply angle and considerably higher for the specimens with 60° interply angle, suggesting more fibre bridging and delamination branching for the latter. This was confirmed by the visual observations during the tests as well as by the photograph presented in Figure 3(a).

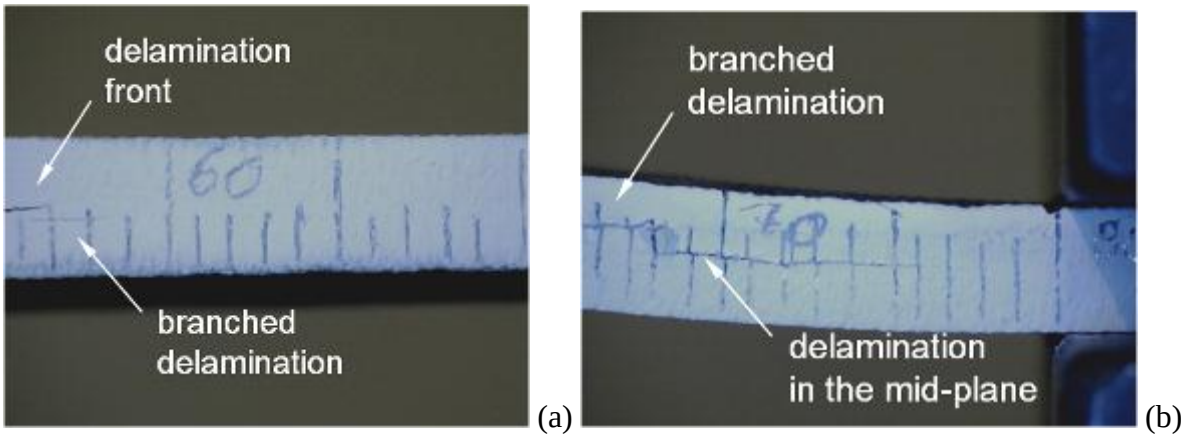

Figure 3 Photographs of delamination branching while testing a specimen with 60° interply angle under **(a)** Mode I and **(b)** Mode II loading

For Mode II loading the experimental results in Figure 2 indicate that for delamination initiation the Mode II apparent fracture toughness increases as the interply angle increases to 20° with a drop recorded for the 60° case. The area method yielded results that indicate an initial drop in Mode II delamination resistance followed by a continuous increase as the interply angle increases to 60°. The area method provides a macroscopic measure of the fracture toughness and includes all mechanisms that occur during fracture. The observed delamination branching at 60° (Figure 3(b)), which will increase the delamination resistance, also supports the increase found in the apparent Mode II values. A similar trend was found for glass fibre filament wound multi-angle composites tested under Mode II on an end notch flexure arrangement [6].

5. Fractographic observations

5.1 Mode I fracture surfaces

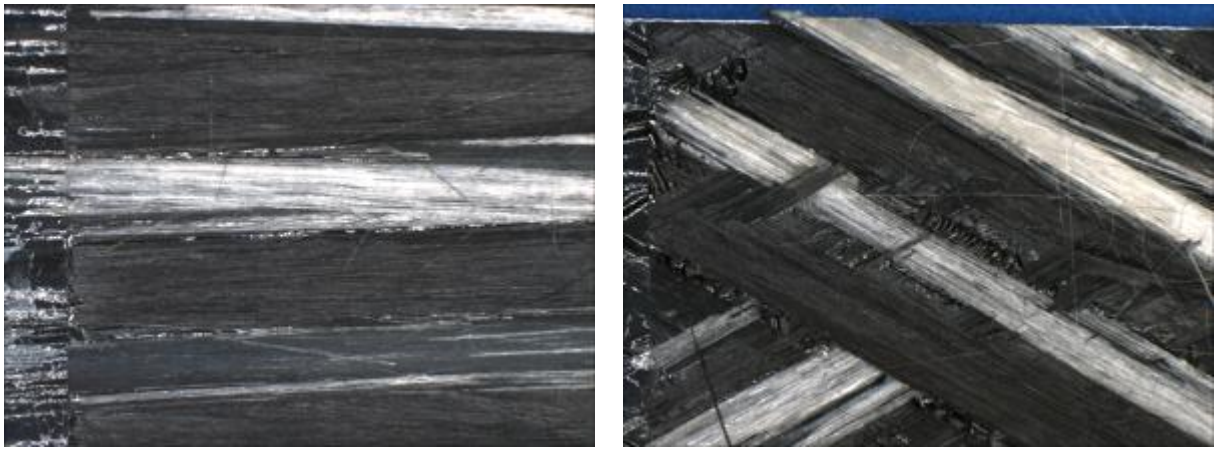

5° **60°**

Figure 4. Mode I fracture surfaces (starter crack on the left).

Mode I fracture surface morphologies versus interply angle at a macroscopic level are shown in Figure 4. At low interply angles the surface was akin to that of a unidirectional laminate [7]. However, as the interply angle increased, wedges of resin-rich regions manifested between the tow cross-over points. At modest angles these were thin but at high interply angles they became quite severe, disrupting the tow microstructure. At low interply angles there was little interaction between the individual tow delaminations. However, as the interply angle increased, individual fibres, and at large angles, entire tows, bridged across the surface. This led to localized multiplane delaminations, which would have enhanced the apparent toughness. These sites tended to have failed cohesively, with the delaminations extending longitudinally along the fibres, and then obliquely into the resin-rich sites, as has been observed in woven materials [8]. The influence of these resin-rich sites seemed to increase with interply angle.

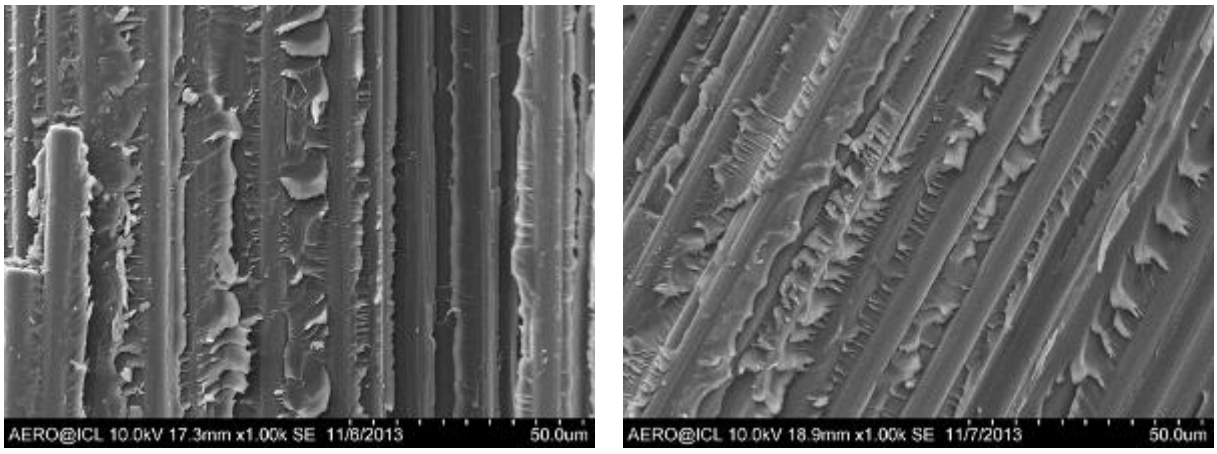

5° **60°**

Figure 5. Mode I fracture surfaces approximately 20mm from the starter crack (lowermost).

Electron micrographs of the typical morphology about 20 mm from the insert tip are shown in Figure 5. The morphology of the 5° was fairly typical of a Mode I surface in a unidirectional

laminate, exhibiting riverlines, matrix cleavage, but there were some shallow cusps, perhaps associated with fibre bridging [7]. As the interply angle increased, the cusps tended to be orientated with the fibres (i.e. not aligned with the overall growth direction), although they also became less symmetric (perhaps associated with a Mode III component). The cusps also became more erect as the interply angle increased, which was consistent with an increase in the local Mode II component.

5.2 Mode II fracture surfaces

Mode II fracture surface morphologies versus interply angle are shown in Figure 6. It was notable that the resin-rich wedges were not as apparent as had been seen on the Mode I fracture surfaces, with the fracture plane just tending to exhibit larger cusps at these sites. Increasingly fracture occurred on both sides of the interply resin layer leaving islands of resin on the fracture surface, potentially increasing fracture energy. In addition, as the interply angle increased, so did the degree of tow overlap and bridging of bundles of fibres.

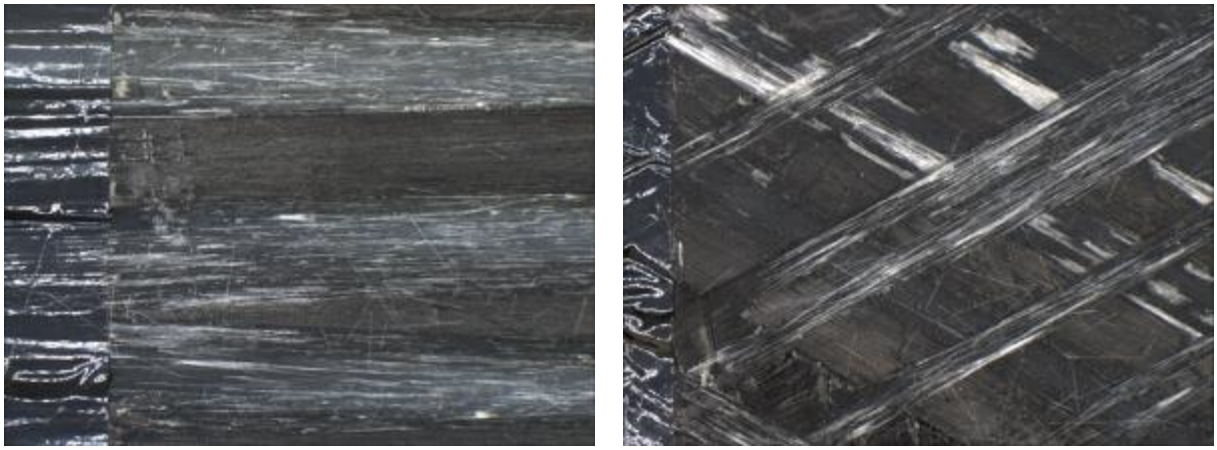

5° **60°**

Figure 6. Mode II fracture surfaces (starter crack on the left).

Electron micrographs of the typical morphology about 20mm from the insert tip are shown in Figure 7.

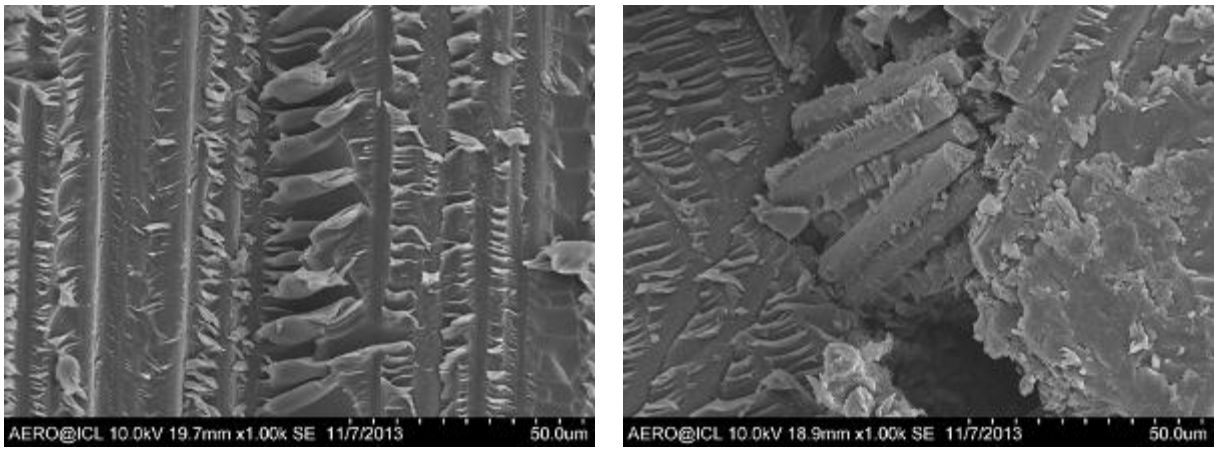

5° **60°**

Figure 7. Mode II fracture surfaces approximately 20mm from the starter crack (lowermost).

The morphology of the 5° was fairly typical of a Mode II surface in a unidirectional laminate, exhibiting cusps and one face being fibre dominated, the other being fibre imprint dominated [7]. The cusps were fairly typical of Mode II. As the interply angle increased, the cusp morphology became more irregular, with crows-feet only on one side (consistent with Mode III component having been present [9]). At high interply angles the cusps were also intersected by deep gouges and tended to be aligned with the tow rather than the specimen direction. At high angles, there was no clearly defined fibre and fibre imprint dominated face. Finally, at high interply angle (60°) there was evidence of fibre microbuckling having developed prior to delamination (i.e. it bounded two delamination directions). The orientation of the microbuckling was consistent with in-plane shear having developed within this tow.

6. Discussion

6.1 Active fracture mechanisms (Mode I)

From Figure 4, the direction of the river lines shows that the resin pockets do not fail first. Fibre bridging also increases with interply angle. From Figure 5, the presence of shear cusps in the neighbouring tow bundles shows a considerable Mode II component to the tow separation. Cusp alignment suggests a degree of local Mode III, which may be caused by local misorientation of the crack plane.

The energy involved in fibre failure has been measured as 91.6 kJ/m2 [10], and the Mode I toughness of pure resin has been measured by the manufacturer as 168 J/m2 [11], a value below all the Mode I toughness values measured in this work. There is no clear trend in measured Mode I values with interply angle, suggesting that the increasing importance of both the highest- and lowest-energy failure mechanisms with increasing interply angle are competing with each other.

6.2 Active fracture mechanisms (Mode II)

Figures 6 and 7 both show fairly pure Mode II growth along the tow. Resin failure at tow junctions is present, but is less important than in Mode I. Tow micro-buckling is present at high interply angles, and can be seen in Figure 7. Changes in local growth direction across the micro-buckles suggest the micro-buckles occur ahead of the delamination. The micro-buckles occur at the position of maximum out-of-plane tow angle where the failed tow crosses an underlying tow. Finally, wide fractures across several fibre imprints at 60° interply angle is evidence of gouging, which has also been observed and described in cross-ply laminates [12].
It is anticipated that resin fracture would be the lowest energy (although it is barely present in the Mode II specimens), followed by Mode II growth along the tow, gouging, and fibre micro-buckling. Gouging and micro-buckling become markedly more important as the interply angle approaches 90°, suggesting a strong increase in the apparent Mode II fracture toughness would be observed.

In the case of Mode II, the trend expected from an investigation of the active mechanisms is in fact present. At interply angles up to 20°, where the primary failure mechanism remains Mode II growth along the tow direction, there is only a weak dependence on the interply angle. However, at an interply angle of 60° there is a strong increase in the apparent fracture toughness, commensurate with the increased importance of the high-energy micro-buckling and gouging mechanisms at this high angle.

7. Conclusions

It is clear from the fractographic analysis that several different fracture processes are active in fracture of these filament-wound specimens: mixed-mode growth along the local tow direction was seen, along with varying proportions of resin brittle failure, fibre bridging, fibre micro-buckling and gouging depending on the loading mode and interply angle. These different fracture processes are associated with different absorbed energies, therefore, as their relative proportions change, the total fracture energy of the specimens will change. The current work shows that, in principle, it should be possible to predict the variation of apparent fracture toughness with interply angle, given the constitutive properties of the components of the composite and a knowledge of the laminate construction. The solution to this problem depends on the development of a mechanistic understanding of each of the processes shown to be active in this work, in order to facilitate prediction of the relative proportions of active processes for each interply angle.

References

[1] J. C. Fish, S. D. Malaznik. Fracture of Double Beam Specimens Containing 90-degree Plies. *Key Engineering Materials*, 121-122, 347-360, 1996

[2] I. Chou, I. Kampara, K. Kageyama, I. Ohsawa. Mode I and Mode II Fracture Toughness Measured Between Differently Oriented Plies in Graphite/Epoxy Composites. *ASTM STP*, 1230, 132-51, 1995

[3] ESIS T4 Protocol. Fibre Composites – The Determination of the Mode II Fracture Resistance, G_{IIc}, of Unidirectional Fibre Composites using the Calibrated End-Loaded Split (C-ELS) Test and an Effective Crack Length Approach, 2008

[4] B. R. K. Blackman, A. J. Kinloch, M. Paraschi. The Determination of the Mode II Adhesive Fracture Resistance, G_{IIc}, of Structural Adhesive Joints: an Effective Crack Length Approach. *Engineering Fracture Mechanics*, 72, 877-897, 2005

[5] S. Giannis, K. Hansen, R.H Martin. Accounting for the R-curve Effects on the Mode I Fatigue Delamination Growth Characterisation of Unidirectional Composites. In *25th Annual Technical Conference of the American Society for Composites / 14th U.S.-Japan Conference on Composites Materials*, 2010

[6] J. F. Silva, P. Vieira, A. B. Morais, A. T. Marques, P. M. S. T. de Castro. Mode II Fracture Toughness of Glass Fibre Reinforced Composites. In *8th Portuguese Conference on Fracture*, 2002

[7] E. S. Greenhalgh. *Failure Analysis and Fractography of Polymer Composites*, Woodhead, London, 2009

[8] J. K. Kim, M. L. Sham. Impact and Delamination Failure of Woven-Fabric Composites. *Composites Science and Technology*, 60(50), 745-761, 2000

[9] C. Canturri, E. S. Greenhalgh, S. T. Pinho, J. Ankersen. Delamination Growth Directionality and the Subsequent Migration Processes – the Key to Damage Tolerant Design. *Composites Part A*, 54, 79-87, 2013

[10] S. T. Pinho, P. Robinson, L. Iannucci. Fracture Toughness of the Tensile and Compressive Fibre Failure Modes in Laminated Composites. *Composites Science and Technology*, 66(13), 2069-2079, 2006

[11] Hexcel Corp. Publication ITA 290. 2010

[12] E. S. Greenhalgh, L. E. Asp, S. Singh. Delamination Resistance, Failure Criteria and Fracture Morphology of 0/90°, 0/5° and 0/90° Ply Interfaces in CFRP. In *5th International Conference on Deformation and Fracture of Composites*, 1999